Investigation of emission properties of Tm^{3+}:Y_2O_3 transparent ceramic

Qing Yi (易 庆)[1,3], Taiju Tsuboi[2], Shengming Zhou (周圣明)[1*], Yosuke Nakai[2], Hui Lin (林 辉)[1], and Hao Teng (滕 浩)[1]

[1]*Shanghai Institute of Optics and Fine Mechanics, Chinese Academy of Sciences, Shanghai 201800, China*

[2]*Faculty of Engineering, Kyoto Sangyo University, Kamigamo, Kita-ku, Kyoto 603-8555, Japan*

[3]*Graduate University of Chinese Academy of Sciences, Beijing 100049, China*

[*]*Corresponding author: zhousm@siom.ac.cn*

Received February 23, 2012; accepted March 28, 2012; posted online July 13, 2012

A transparent and emitting ceramic of Y_2O_3 doped with 6% Tm^{3+} ions is fabricated by vacuum sintering with ZrO_2. Absorption, photoluminescence (PL), and PL excitation (PLE) spectra are investigated in a spectral range of 200 to 2 100 nm at various temperatures between 296 and 12 K. Intense emission band appears at 450 to 465 nm in the visible range. Near-infrared emission bands are observed at 1 200 to 1 300 nm and 1 400 to 1 550 nm, with intense peaks at 1 270, 1 450, and 1 523 nm. The luminescence mechanisms and potential applications of the emissions are discussed with the help of Judd-Ofelt theory and PLE spectra.

OCIS codes: 160.4670, 160.5690.

doi: 10.3788/COL201210.091602.

Cubic Y_2O_3 material has been widely investigated as a host material for accommodating rare earth ions. The advantages of yttria (yttrium oxide) host material include high refractive index, low phonon energies, and wide optically transparent range. More importantly, the thermal conductivity of yttria is larger than that of $Y_3A_{15}O_{12}$[1,2]. However, the high melting point of 2 430 °C and phase transformation at approximately 2 280 °C of Y_2O_3 make it considerably difficult to grow single Y_2O_3 crystals by conventional methods. On the contrary, transparent ceramics are much easier to produce than single crystals because of much lower processing temperatures.

Since the first demonstration of Nd:YAG ceramic laser in 1995 by Ikesue[3], transparent ceramic materials have received a wide attention[4−7]. Transparent ceramics have optical properties comparable to single crystal, but with better mechanical properties. Additionally, fabrication of materials with big size is much easier for ceramics than for single crystals. These advantages make transparent ceramics attractive for laser media, fluorescent materials, and window materials.

In this letter, a Tm^{3+}-doped Y_2O_3 transparent ceramic is synthesized by vacuum sintering with ZrO_2. We found that Zr^{4+} ions can suppress the grain boundary migration, resulting in a uniform microstructure. The Judd-Ofelt theory is applied to analyze the observed luminescence of Tm^{3+} ions in Y_2O_3 ceramic. Although Tm^{3+} luminescence has been reported on Tm^{3+}-doped Y_2O_3 single crystals[8−10], the measurements were made at room temperature, not at low temperatures. We report the photoluminescence (PL) and PL excitation (PLE) spectra of Tm^{3+}-doped Y_2O_3 ceramic at temperatures from 12 to 295 K. The luminescence mechanisms and the potential of the laser application are also discussed.

High-purity commercial powders of Y_2O_3(99.99%), Tm_2O_3(99.99%), and ZrO_2(99.99%) were used as starting materials. The powders were weighed according to the stoichiometry of $(Zr_{0.03}Tm_{0.06}Y_{0.91})_2O_3$, then ball-milled in alcohol for 20 h. The obtained slurries were dried and then ground with a pestle. The mixed powders were sieved through a 200 mesh screen. Next, the powders were dry-pressed in a stainless steel mold into discs 15 mm in diameter and 3 mm in height under low pressure. The discs were cold-isostatic-pressed under 250 MPa. The pressed discs were calcined at 600 to 1 000 °C for 2 h. Eventually, transparent ceramics were obtained after vacuum sintering at 1 800 °C for 20 h with a vacuum degree of 1×10^{-3} Pa. The polished discs were etched in H_3PO_4 at 80 °C for 3 min for the observation of the microstructures. The synthesized ceramics were polished for optical measurements.

The optical transmittances were obtained by a UV/VIS/NIR spectrophotometer (V-900, JASCO, Japan). The PL spectra in the temperature range of 12 to 295 K and PLE spectra at 12 and 295 K were measured with a spectrophotometer (Fluorolog-3, Spex, USA). Infrared PL spectra were measured in a spectral range of 800 to 1 600 nm using a liquid-nitrogen-cooled InGaAs photodiode (DSSX-IGA010I, Jobin-Yvon, France).

Figure 1 shows the microstructure of the ceramic observed using a Leitz optical microscope. As seen in the photograph, the microstructure is uniform and no pores

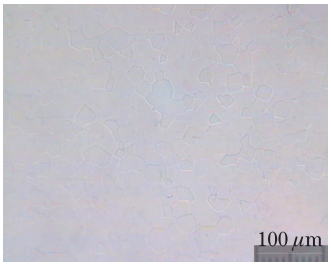

Fig. 1. Microstructure of Tm_{3+}-doped Y_2O_3 ceramic.

can be observed in the ceramic. The average grain size was determined to be 22 μm by multiplying the average interpreting grain size with a correlation factor of 1.56[11].

The mass transfer mechanism in the sintering process of Y_2O_3 ceramic has been investigated by Chen *et al.*[12]. The diffusion of Y^{3+} interstitials is considered as the controlling step of the grain boundary migration. When the Zr^{4+} ions were introduced into the Y_2O_3 lattice, the following defect reaction occurred

$$2ZrO_2 \xrightarrow{Y_2O_3} 2Zr_Y + 3O_o + O_i''. \quad (1)$$

The concentration of Y^{3+} interstitial decreases with the increasing of the O^{2-} interstitial concentration[12]. Thus, the doping of Zr^{4+} leads to increase of O^{2-} interstitials, followed by decrease of Y^{3+} interstitials, resulting in decrease of the mobility of the grain boundary. The lower grain boundary mobility leads to an easier elimination of pores from the grain boundary. As a result, a uniform microstructure is obtained. Figure 2 displays the transmittance spectrum of the ceramic, which shows a transmittance of 76.3% at 1 μm. From the picture shown in inset of Fig. 2, the transparency of the ceramic can be recognized clearly. Several sharp lines are present in the transmittance spectrum, which are due to the doped Tm^{3+} ions.

Transparency of the ceramic is also confirmed by the absorption spectrum of Fig. 3. Sharp intense absorption lines are observed at 360, 463, 684, 796, 1 207, and 1 631 nm. The absorption spectrum of Tm^{3+} ions doped in Y_2O_3 single crystal at 600 to 2 200 nm has been presented by Mun *et al.*[8]. Their spectrum is quite similar to that in Fig. 3, indicating that the Tm^{3+} ions in the Y^{3+} site with C2 symmetry in the single crystal[9] are also present in our ceramic. The energy level diagram of Tm^{3+} ion in the Y_2O_3 ceramic shown in Fig. 4 was obtained from the absorption spectrum. Intense absorption due to the Y_2O_3 host arises from approximately 350 nm. Using the Judd-Ofelt theory, the measured absorption line strengths for the Tm^{3+} bands were calculated by

$$S_{\mathrm{mea}}(J \to J') = \frac{3hc(2J+1)}{8\pi^3 e^2 N_0} \frac{9n}{(n^2+2)^2} \frac{\Gamma}{\overline{\lambda}}, \quad (2)$$

where the c and h represent the speed of the light and the Planck's constant, respectively. Here, N_0 means the number density of Tm^{3+} ions and n refers to the refractive index of the sample. $\overline{\lambda}$ represents the average wavelenth of $J - J'$ transition. J and J' represent the total angular momentum quantum number. τ meas $\frac{1}{0.43N_oL}\int \mathrm{OD}(\lambda)\mathrm{d}\lambda$, where L means the orbital angular momentum quantum number, and the $\mathrm{OD}(\lambda)$ means the optical density which could be obtained during absorption spectrum measurement. e means the charge quality of an electron. The calculated absorption line strengths were derived from

$$S_{\mathrm{cal}}(J \to J') = \sum_{t=2,4,6} \Omega_{\mathrm{tq}} |\langle (S,L)J||U^{(t)}||(S'L')J'\rangle|^2, \quad (3)$$

where $|\langle (S,L)J||U^{(t)}||(S'L')J'\rangle|^2$ are the double-reduced matrix elements of unit tensor operators[13], which are independent of the host matrix. By least-squares fitting of the calculated line strengths to the measured line strengths, the Judd-Ofelt parameters $\Omega_{2,4,6}$ were determined to be 4.57×10^{-20}, 0.97×10^{-20}, and 0.94×10^{-20}. Using these parameters, the spontaneous emission line strengths, transition probabilities, branching ratios, and radiative lifetimes in Tm:Y_2O_3 ceramic were calculated (see Table 1). The detailed calculation processes were described in Refs. [10, 14-17].

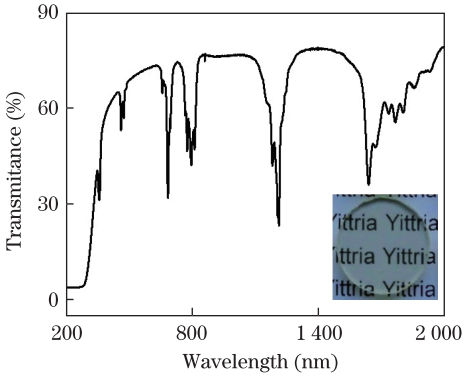

Fig. 2. Transmittance spectrum of Tm_{3+}-doped Y_2O_3 ceramic. Inset shows a picture of the circle-shaped ceramic placed on a paper.

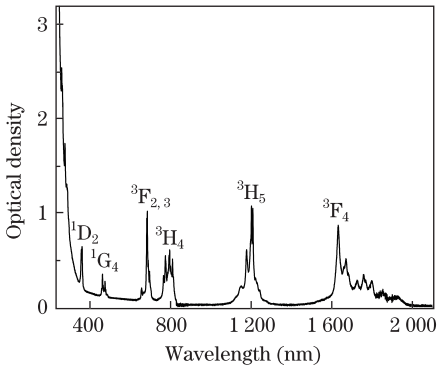

Fig. 3. Absorption spectrum of Tm_{3+}-doped Y_2O_3 ceramic. The excited state responsible for each of the absorption bands is indicated.

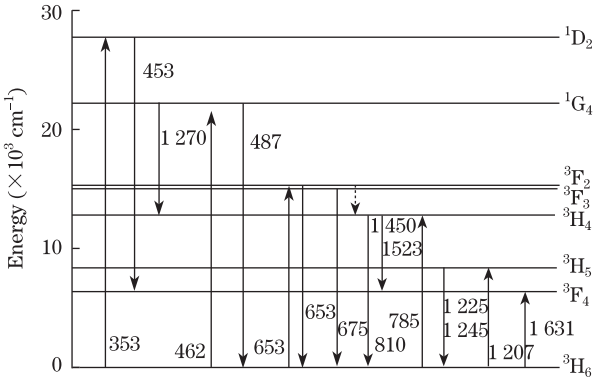

Fig. 4. Energy level diagram of Tm_{3+} ions in Y_2O_3 host material, which was obtained from the absorption spectrum, and the level assignment for the observed emission bands. The number (e.g., 453) refers to the emission (e.g., 453-nm emission). The dotted arrow indicates the non-radiative multiphonon transitions.

Table 1. Calculated Emission Transition Probability, Branching Ratio, and Radiative Lifetime of Tm^{3+} Ion in Y_2O_3 Ceramic

Radiative Transition	Average Emission Wavelength (nm)	Electric-dipole Transition Probability A_{ed} (s^{-1})	Magnetic-dipole Transition Probability A_{ed} (s^{-1})	Branching Ratio (%)	Radiative Lifetime τ (ms)
$^1D_2 \rightarrow {}^1G_4$	1 503.9	294.90		0.63	0.02
$^3F_2$	785.5	1 217.86		2.73	
$^3F_3$	751.4	1 926.08		4.32	
$^3H_4$	654.5	2 861.19		6.14	
$^3H_5$	512.0	125.39		0.27	
$^3F_4$	452.5	31 468.85		67.53	
$^3H_6$	358.1	8 527.62		18.30	
$^1G_4 \rightarrow 3F_2$	1 644.2	17.07		0.49	0.29
$^3F_3$	1 501.6	64.68		1.98	
$^3H_4$	1 158.9	377.69		11.88	
$^3H_5$	776.4	990.81		32.43	
$^3F_4$	647.2	209.31		6.39	
$^3H_6$	469.9	1 623.60		46.92	
$^3F_2 \rightarrow 3F_3$	17 310.5	0.02		0.00	0.43
$^3H_4$	3 925.7	28.52		1.22	
$^3H_5$	1 471.0	260.60		11.18	
$^3F_4$	1 067.3	1 198.06		51.42	
$^3H_6$	658.0	844.37		36.24	
$^3F_3 \rightarrow {}^3H_4$	5 077.1	5.35		0.17	0.32
$^3H_5$	1 607.5	548.41		17.41	
$^3F_4$	1 137.4	81.31	125.85	4.52	
$^3H_6$	684.0	2 450.01		77.78	
$^3H_4 \rightarrow {}^3H_5$	2 352.3	22.65	17.73	1.47	0.46
$^3F_4$	1 465.7	159.50		8.30	
$^3H_6$	790.5	1 953.45		90.44	
$^3H_5 \rightarrow {}^3F_4$	3 889.1	10.84		2.46	2.23
$^3H_6$	1 190.6	351.80	112.15	97.44	
$^3F_4 \rightarrow {}^3H_6$	1 715.9	369.95		100.00	2.70

Figures 5(a) and (b) show the PL spectra of the ceramic excited at 361 nm at various temperatures between 12 and 295 K in the spectral ranges of 420 to 870 nm and 440 to 500 nm, respectively. An intense emission band with peak around 453 nm can be observed, whereas very weak emission bands with peaks at 653, 675, and 810 nm can be observed by the $^1D_2$ excitation at 361 nm. From comparison with the absorption spectrum, the 653 to 675 nm and 810 nm emission bands are attributable to the electronic transitions from the $^3F_{2,3}$ and $^3H_4$ states to the ground state $^3H_6$, respectively. Of the blue emission bands at 445 to 490 nm, the emission band appearing at 445 to 465 nm is attributable to the transition $^1D_2 \rightarrow {}^3F_4$, whereas the emission band at 480 to 495 nm with the highest peak at 487 nm is ascribed to the transition $^1G_4 \rightarrow {}^3H_6$. The former band intensity is higher than the latter band intensity (see Fig. 5(b)). This result is consistent with the calculation that the $^1D_2 \rightarrow {}^3F_4$ transition has a much higher electric dipole transition probability than the $^1G_4 \rightarrow {}^3H_6$ transition (see Table 1). The assignment of the 480 to 495 nm emission band to the $^1G_4 \rightarrow {}^3H_6$ transition was confirmed from observation of the 480 to 495 nm emission by $^1G_4$ excitation at 462 nm. The intense blue emission under ultraviolet excitation, especially the emission around 453 nm, suggests the application of Tm:Y_2O_3 ceramic in white LED packaging with an ultraviolet chip, where Tm:Y_2O_3 could be used as one of the three-color sources.

The electric dipole transition probability is 31468 s^{-1} for the $^1D_2 \rightarrow {}^3F_4$ transition responsible for the 453-nm

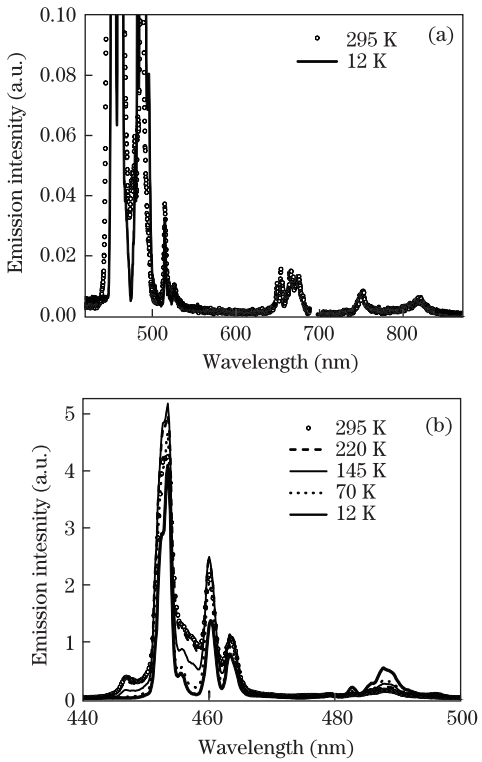

Fig. 5. Emission spectra of Tm_{3+} ions in Y_2O_3 ceramic excited at 361 nm at various temperatures between 12 and 295 K, in the spectral ranges of (a) 420 to 870 nm and (b) 440 to 500 nm.

emission, 844 s^{-1} for the $^3F_2 \rightarrow ^3H_6$ transition responsible for the 653-nm emission, 2 450 s^{-1} for the $^3F_3 \rightarrow ^3H_6$ transition responsible for the 675-nm emission, and 1 953 s^{-1} for the $^3H_4 \rightarrow ^3H_6$ transition responsible for the 810-nm emission (see Table 1). The $^1D_2 \rightarrow ^3F_4$ transition has a much higher transition probability than the other transitions. From this Judd-Ofelt calculated transition probabilities, we can understand the reason the intensities of the emission bands around 653, 675, and 810 nm are much weaker than the intensity of the emission band around 453 nm.

No clear temperature dependence could be observed for the peak emission intensity at 453 nm, as plotted in Fig. 6. However, the weak emission sideband at 446 nm was found to have temperature dependence (i.e., the 446-nm-emission intensity decreases with decreasing temperature from 295 K and finally disappears at 12 K) (see Fig. 5(b)). The decrease of the 446-nm emission is suggested to due to the decrease of thermal population in the excited state responsible for the 446-nm emission, which is located at higher level than the excited state responsible for the main 453-nm emission. The weak temperature dependence of the peak emission intensity indicates that the material has a good operation stability under different working temperatures while used as LED packaging material.

The PL spectra at 12 K in the range of 800 to 1 600 nm are shown in Fig. 7, where the ceramic was excited at 361, 465, 683, and 785 nm to give rise to the excitation into the $^1D_2$, $^1G_4$, $^3F_{2,3}$, and $^3H_4$ states, respectively. Two emission bands could be observed at 1 200 to 1 300 nm and 1 400 to 1 560 nm, with intense peaks at 1 270, 1 450, and 1 523 nm. Regarding the 1 400 to 1 560 nm band, the same emission line-shape was obtained for the four different excitation wavelengths, indicating the various emission peaks in the 1 400 to 1 560 nm emission band arises from the same transition. Regarding the 1 200- to 1 300-nm emission band, we determined that (1) the 361- and 465-nm excitations give the same emission line shape; (2) the line shape is different from that obtained from the 683- and 785-nm excitations; and (3) the 683- and 785-nm excitations give the same line shape that consists of three peaks at 1 216, 1 225, and 1 245 nm. The three peaks could not be observed at room temperature, but could be observed at low temperature, such as 12 K (see Fig. 8).

Figure 9 shows the PLE spectra for the 1 270- and 1 450-nm emissions. The 1 270-nm emission appears by the $^1D_2$ and $^1G_4$ excitations at 358 and 462 nm, respectively; however, it never appears by the $^3F_{2,3}$ and $^3H_4$ excitations at 685 and 776 nm, respectively. Therefore, considering the energy level diagram of Tm^{3+}, the 1 270-nm emission is attributed to the $^1G_4 \rightarrow ^3H_4$ transition as shown in Fig. 4. The branching ratio of this transition is 11.88%, supporting the appearance of this radiative transition. The 1 400- to 1 560-nm emission band is generated by all the excitations at approximately 358, 462, 685, and 776 nm. From the energy level diagram derived from the absorption spectrum, this emission is attributable to the $^3H_4 \rightarrow ^3F_4$ transition (see Fig. 4).

The PL spectra of Tm^{3+} ions in Y_2O_3 ceramic observed in visible and near-infrared region are quite similar to the spectra of Tm^{3+} ions in Y_2O_3 single crystals[9]. This similarity indicates that Tm^{3+} ions locate at Y^{3+} sites in the Y_2O_3 lattice in the ceramic state, as in the case of single crystal.

The stimulated emission cross-section was calculated to be 1.41×10^{-20} and 7.2×10^{-21} cm^2 for the 1 270- and 1 450-nm emissions, respectively, whereas the absorption cross-section was calculated to be 1.5×10^{-21} and 6.2×10^{-21} cm^2 for the 465- and 683-nm absorption bands. The excitation at 361 and 465 nm gives the 1 270- and 1 450-nm emissions, as seen in Fig. 7. The 1 270-nm emission intensity is observed to be higher than the 1 450-nm emission intensity. This observation is consistent with the calculation of the stimulated emission cross-sections for the two emissions. The absorption cross-section is larger for the 683-nm band than for the 465-nm band. This phenomenon suggests a possibility of laser oscillation at 1 450 nm by pumping with light around 683 nm.

The 1 450-nm laser oscillation is due to the four-level laser system, which consists of the $^3H_6$ ground state, the $^3F_3$ state as a pumping state, the $^3H_4$ state as emitting state, and the $^3F_4$ state as final state. The relaxation from the $^3F_3$ state to the $^3H_4$ state is fast due the following reason. The energy gap of the $^3F_3$ and $^3H_4$ state is approximately 1 900 cm^{-1}, whereas the maximum phonon energy of Y_2O_3 is 591 cm^{-1}[18]. Therefore, the non-radiative multi-phonon transition occurs easily from the $^3F_3$ level to the $^3H_4$ level, leading to (1) the suppression of the radiative transition from the $^3F_3$ level to the other lower levels

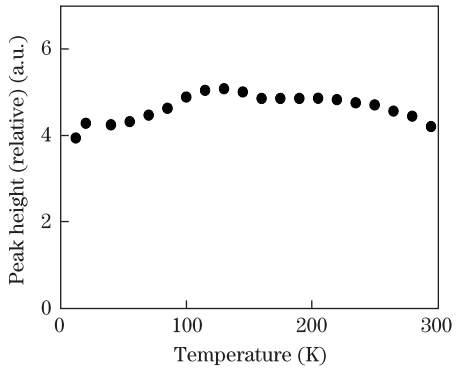

Fig. 6. Temperature dependence of the 453-nm emission peak height.

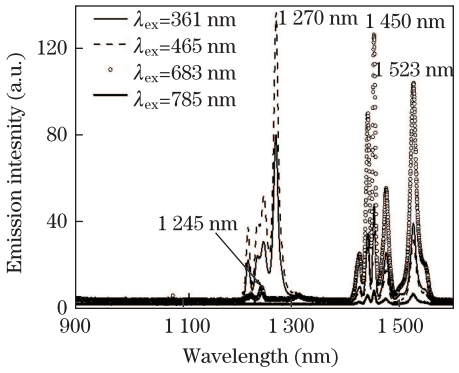

Fig. 7. Near-infrared photoluminescence spectra of Tm3+ ions in Y_2O_3 ceramic under 361-, 465-, 683-, and 785-nm excitations at 12 K.

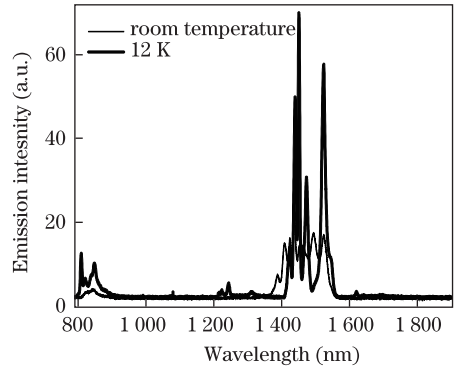

Fig. 8. Near-infrared emission spectra of Tm_{3+} ions in Y_2O_3 ceramic excited at 683 nm at room temperature and 12 K.

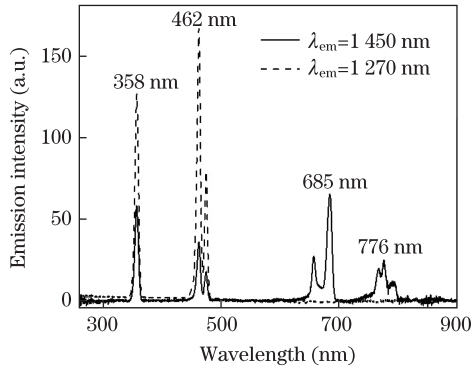

Fig. 9. Photoluminescence excitation spectra for 1 270- and 1 450-nm emissions of Tm_{3+} ions in Y_2O_3 ceramic at 12 K.

including the ground state $^3H_6$ and (2) enhancement of the population in the emitting $^3H_4$ state. This laser system is superior to the three-level 1.5-μm-laser system of Er^{3+}. However, the longer lifetime of the terminal $^3F_4$ state (2.7 ms, as shown in Table 1) compared to that of the upper $^3H_4$ state (0.46 ms) leads to a self-terminating laser operation. This issue can be solved by co-doping Tb^{3+} and Tm^{3+} ion, which decreases the lifetime of the terminal $^3F_4$ state, as suggested by Ermeneux *et al.*[10]. The concentration of Tm^{3+} ions is 6% in the present Y_2O_3 ceramic. Because such a high doping concentration is easier to achieve in ceramics than in single crystals[3], the co-doping of Tm^{3+} and Tb^{3+} in Y_2O_3 ceramic will be easy to realize.

As seen in Fig. 8, the room temperature spectrum shows a broad emission band around 1 450 nm with a large full-width at half-maximum (FWHM) of 135 nm. This result indicates that the Tm^{3+}:Y_2O_3 ceramic is beneficial for the tunable laser oscillation or ultrashort pulse laser oscillation at room temperature.

In conclusion, a transparent ceramic of Y_2O_3 doped with Tm^{3+} has been fabricated by vacuum sintering with ZrO_2. The grain boundary is clean and the average grain size is 22 μm. The PL spectra in a spectral range of 400 to 1 600 nm were investigated at various temperatures between 12 and 295 K. The level assignment was made for all the observed emission bands from the PL spectra under various excitations, the PLE spectra, and the transition probabilities calculated by the Judd-Ofelt theory. We confirmed that Tm^{3+} ions locate at Y^{3+} sites in Y_2O_3 lattice in the ceramic state, as in the case of single crystal. A highly intense 1 450-nm emission band was observed under the 683-nm excitation. The absorption cross-section at 683 nm and stimulated emission cross-section at 1 450 nm were calculated to be 6.2×10^{-21} and 7.2×10^{-21} cm^2, respectively. This result indicates that Tm^{3+}:Y_2O_3 ceramic is a candidate of laser gain material for 1 450-nm oscillation operated by the four-level laser system.

This work was supported by the National Natural Science Foundation of China (Nos. 51172254 and 60990311), the Special Funds for Major State Basic Research Project of China (No. 2011CB301900), and the Science and Technology Commission of Shanghai Municipality (No. 10JC1415700).

References

1. X. R. Hou, S. M. Zhou, Y. K. Li, and W. J. Li, Opt. Mater. **32,** 1435 (2010).
2. J. R. Lu, J. H. Lu, T. Murai, K. Takaichi, T. Uematsu, K. Ueda, H. Yagi, T. Yanagitani, and A. A. Kaminskii, Jpn. J. Appl. Phys. **40,** 1277 (2001).
3. A. Ikesue and Y. L. Aung, Nat. Photonics **2,** 721 (2008).
4. Y. B. Wang, B. S. Wang, Y. Bao, J. L. Xu, S. Song, X. J. Peng, Z. Y. Xu, W. B. Liu, and Y. B. Pan, Chin. Opt. Lett. **8,** 1144 (2010).
5. H. Cai, J. Zhou, H. Zhao, Y. Qi, Q. Lou, J. Dong, and Y. Wei, Chin. Opt. Lett. **6,** 852 (2008).
6. Y. Qi, Q. Lou, H. Ma, and J. Dong, Chin. Opt. Lett. **3,** 89 (2005).
7. B. Jiang, T. Huang, Y. Wu, W. Liu, and Y. Pan, Chin. Opt. Lett. **7,** 505 (2009).
8. J. H. Mun, A. Jouini, A. Novoselov, Y. Guyot, A. Yoshikawa, H. Ohta, H. Shibata, Y. Waseda, G. Boulon, and T. Fukuda, Opt. Mater. **29,** 1390 (2007).
9. Y. Guyot, R. Moncorgd, L.D. Merkle, A. Pinto, B. McIntosh, and H. Verdun, Opt. Mater. **5,** 127 (1996).
10. F. S. Ermeneux, C. Goutaudier, R. Moncorgé, M. T. Cohen-Adad, M. Bettinelli, and E. Cavalli, Opt. Mater. **8,** 83 (1997).
11. R. L. Fullman, Trans. Am. Instit. Min. Metal. Eng. **197,** 1267 (1953).
12. P. L. Chen and I. W. Chen, J. Am. Ceram. Soc. **79,** 1801 (1996).
13. W. T. Carnall, P. R. Fields, and B. G. Wybourne, J. Chem. Phys. **42,** 3797 (1965).
14. B. M. Walsh, N. P. Barnes, and B. D. Bartolo, J. Appl. Phys. **83,** 2772 (1998).
15. C. Y. Tu, J. F. Li, Z. J. Zhu, Z. Q. Chen, Y. Wang, and B. C. Wu, Opt. Commun. **227,** 383 (2003).
16. D. C. Zhou, R. F. Wang, Z. W. Yang, Z. G. Song, Z. Y. Yin, and J. B. Qiu, J. Non-Crystal. Solids **357,** 2409 (2011).
17. R. Xu, Y. Tian, L. Hu, and J. Zhang, Appl. Phys. B **104,** 839 (2011).
18. E. Husson, C. Proust, P. Gillet, and J. P. Itie, Mater. Res. Bull. **34,** 2085 (1999).